Inorganic Chemistry

Article

pubs.acs.org/IC

# Effects of Proton Acceptors on Formation of a Non-Heme Iron(IV)−Oxo Complex via Proton-Coupled Electron Transfer

Yusuke Nishida,[†] Yuma Morimoto,[†] Yong-Min Lee,[‡] Wonwoo Nam,*[,‡] and Shunichi Fukuzumi*[,†,‡]

[†]Department of Material and Life Science, Graduate School of Engineering, Osaka University, ALCA, Japan Science and Technology (JST), Suita, Osaka 565-0871, Japan,

[‡]Department of Bioinspired Science, Ewha Womans University, Seoul 120-750, Korea

Supporting Information

**ABSTRACT:** Rates of formation of a non-heme iron(IV)−oxo complex, $[Fe^{IV}(O)(N4Py)]^{2+}$ (N4Py = *N*,*N*-bis(2-pyridylmethyl)-*N*-bis(2-pyridyl)methylamine), via electron-transfer oxidation of $[Fe^{III}(OH)(N4Py)]^{2+}$ in acetonitrile (MeCN) containing $H_2O$ (0.56 M) were accelerated as much as 390-fold by addition of proton acceptors such as $CF_3COO^-$, $TsO^-$ ($p$-$MeC_6H_4SO_3^-$), $NsO^-$ ($o$-$NO_2C_6H_4SO_3^-$), $DNsO^-$ (2,4-$(NO_2)_2C_6H_3SO_3^-$), and $TfO^-$ ($CF_3SO_3^-$). The acceleration effect of proton acceptors increases with increasing basicity of the proton acceptors. The one-electron oxidation potential of $[Fe^{III}(OH)(N4Py)]^{2+}$ was shifted from 1.24 to 0.96 V vs SCE in the presence of $TsO^-$ (10 mM). The electron-transfer oxidation of $Fe^{III}$−OH complex was coupled with the deprotonation process by proton acceptors in which deuterium kinetic isotope effects were observed when $H_2O$ was replaced by $D_2O$.

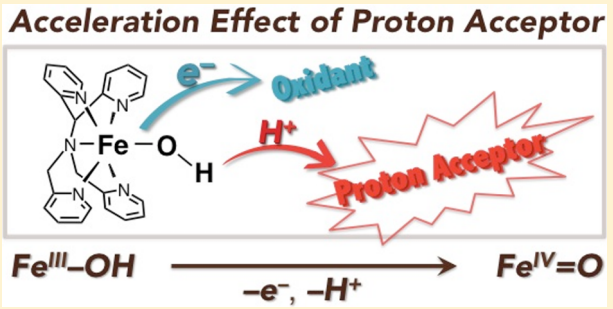


## INTRODUCTION

High-valent metal−oxo species ($M^{(n+2)+}$=O) have been investigated intensively because of their importance as common reactive species in various kinds of oxidation reactions in chemical and biological redox processes, i.e., hydroxylation, chlorination, and desaturation of aliphatic C−H bonds, epoxidation, sulfoxidation, and water oxidation.[1−4] In parallel with studies on the reactivity, formation processes of $M^{(n+2)+}$=O have also merited special attention.[2−7] Metalloenzymes are known to generate $M^{(n+2)+}$=O under mild conditions. In oxidation by enzymes represented by Cytochrome P450 and taurine/$\alpha$-ketoglutarate dioxygenase (TauD), dioxygen ($O_2$) is employed as a terminal oxidant as well as an oxygen source, where $O_2$ is activated through a two-electron reduction and protonations (eq 1)[2,5,6]

$$Fe^{n+} + O_2 + 2e^- + 2H^+ \rightarrow Fe^{(n+2)+}{=}O + H_2O \quad (1)$$

In contrast to reductive activation of $O_2$, the oxygen-evolving complex (OEC), consisting of manganese and calcium ions in photosystem II (PSII), employs a different method to produce the manganese(V)−oxo ($Mn^V{\equiv}O$) complex (Scheme 1), which is regarded as oxidative activation of water responsible for the earth's oxygen and solar energy storage.[7−10]

In the OEC, the $Mn^V{\equiv}O$ complex is produced by stepwise one-electron oxidations of the manganese−aqua ($Mn^{III}$−$OH_2$) complex (eqs 2 and 3), which are key mechanistic steps prior to $O_2$ evolution.[7]

$$Mn^{III}{-}OH_2 - e^- - H^+ \rightarrow Mn^{IV}{-}OH \quad (2)$$

$$Mn^{IV}{-}OH - e^- - H^+ \rightarrow Mn^{V}{\equiv}O \quad (3)$$

Formation of $M^{(n+2)+}$=O through stepwise oxidations of the corresponding low-valent metal−hydroxo or −aqua complex has attracted increasing attention associated with increasing demand for water-oxidation catalyst.[11] This is also important in the development of environmentally benign oxidation processes.[12−17]

With regard to the thermodynamics of formation of $M^{(n+2)+}$=O, the redox potentials between $M^{(n+1)+}$−OH and $M^{(n+2)+}$=O have been shown to be dependent on the pH value of solution.[18] The kinetics as well as thermodynamics of formation of $M^{(n+2)+}$=O via proton-coupled electron transfer (PCET) may also be affected by the presence of proton acceptors (PA) as seen in PSII, where a conjugate base of asparagine acid helps in deprotonation of OEC (Scheme 1).[9] However, to the best of our knowledge, the effects of PA on the kinetics of formation of $M^{(n+2)+}$=O via PCET have yet to be clarified.[19,20]

We report herein remarkable acceleration effects of PA on the rates of formation of a non-heme iron(IV)−oxo complex, $[Fe^{IV}(O)(N4Py)]^{2+}$ (N4Py = *N*,*N*-bis(2-pyridylmethyl)-*N*-bis(2-pyridyl)methylamine), via PCET oxidation of the corresponding iron(III)−hydroxo complex, $[Fe^{III}(OH)(N4Py)]^{2+}$.[21] Detailed study on the kinetics and thermodynamics provides valuable insights into the PCET mechanism.

**Received:** November 24, 2012
**Published:** March 4, 2013

   dx.doi.org/10.1021/ic302573x | *Inorg. Chem.* 2013, 52, 3094−3101

**Scheme 1. Hypothetical Representation of Conversion from the *S3 State to the S4 State in OEC**

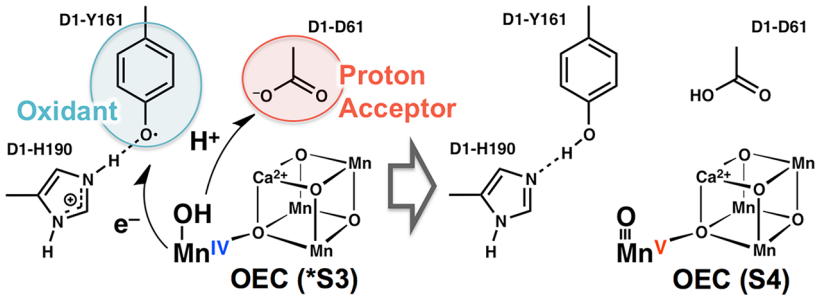


**Scheme 2. Formation of $[Fe^{IV}(O)(N4Py)]^{2+}$ via Stepwise Oxidation of $[Fe^{II}(NCMe)(N4Py)]^{2+}$ in the Presence of Water**

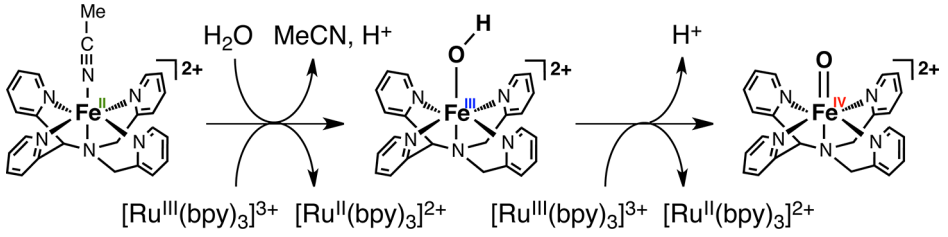


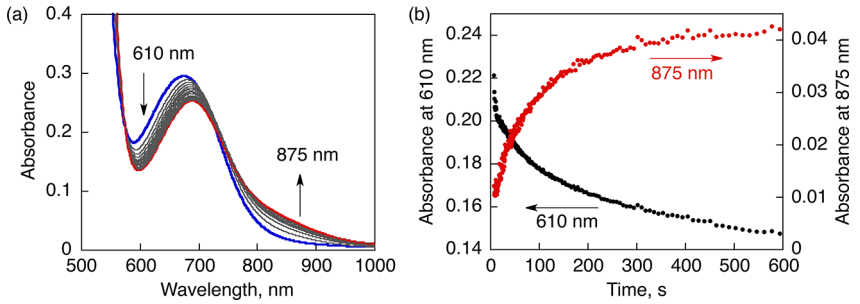


**Figure 1.** (a) Spectral change observed in PCET oxidation of $[Fe^{III}(OH)(N4Py)]^{2+}$ (0.50 mM) with $[Ru^{III}(bpy)_3]^{3+}$ (0.50 mM) in the presence of $TsO^-$ ($p$-$MeC_6H_4SO_3^-$) (10 mM) and 1 vol % of $H_2O$ (0.56 M) in MeCN at 298 K. (b) Time courses of the spectral changes monitored at 610 (black) and 875 nm (red) due to decay of $[Ru^{III}(bpy)_3]^{3+}$ and formation of $[Fe^{IV}(O)(N4Py)]^{2+}$, respectively.

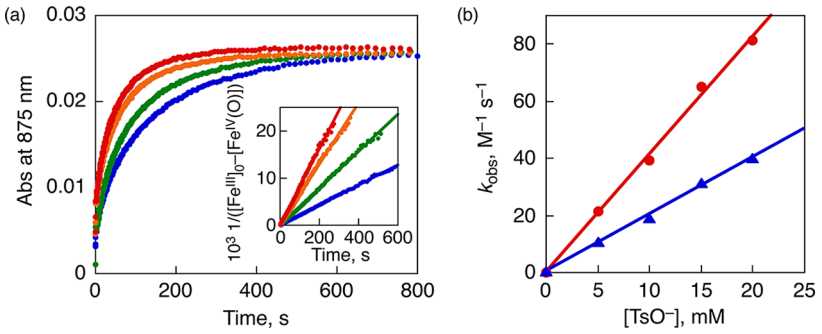


**Figure 2.** (a) Time profiles of absorption change at 875 nm due to the rise of $[Fe^{IV}(O)(N4Py)]^{2+}$ in ET from $[Fe^{III}(OH)(N4Py)]^{2+}$ (0.50 mM) to $[Ru^{III}(bpy)_3]^{3+}$ (0.50 mM) in the presence of $TsO^-$ (blue, 5.0 mM; green, 10 mM; orange, 15 mM; red, 20 mM) and 1 vol % of $H_2O$ (0.56 M) in MeCN at 298 K. (Inset) Second-order plots of the time profiles. (b) Plots of pseudo-second-order rate constants ($k_{obs}$) for reaction of $[Fe^{III}(OH)(N4Py)]^{2+}$ with $[Ru^{III}(bpy)_3]^{3+}$ vs $[TsO^-]$ in the presence of $H_2O$ (0.56 M) (red) or $D_2O$ (0.56 M) (blue).

## RESULT AND DISCUSSION

When 1 equiv of $[Ru^{III}(bpy)_3]^{3+}$ was added into an MeCN solution of $[Fe^{II}(NCMe)(N4Py)]^{2+}$ (0.50 mM), electron transfer from $[Fe^{II}(NCMe)(N4Py)]^{2+}$ to $[Ru^{III}(bpy)_3]^{3+}$ occurred to produce $[Fe^{III}(NCMe)(N4Py)]^{3+}$ and $[Ru^{II}(bpy)_3]^{2+}$. Then, 1 vol % of $H_2O$ (0.56 M) and $TsO^-$ ($p$-$MeC_6H_4SO_3^-$; 10 mM) were added into the resulting solution. Formation of $Fe^{III}$ species was confirmed by EPR, and the signals around $g$ = 4.2 and $g$ = 2.40, 2.17, 1.92 are assigned to $[Fe^{III}(OH)(N4Py)]^{2+}$ (Figure S1, Supporting Information).[22] Further addition of another equivalent of $[Ru^{III}(bpy)_3]^{3+}$ into the solution gave $[Fe^{IV}(O)(N4Py)]^{2+}$ (86% yields) (Scheme 2) as shown in Figure 1a. In the reaction of $[Fe^{III}(OH)(N4Py)]^{2+}$ with $[Ru^{III}(bpy)_3]^{3+}$, decay of the absorption band due to $[Ru^{III}(bpy)_3]^{3+}$ coincides with the rise of the absorption band due to $[Fe^{IV}(O)(N4Py)]^{2+}$ (Figure 1b). Formation of the iron(IV)−oxo complex was also


dx.doi.org/10.1021/ic302573x | Inorg. Chem. 2013, 52, 3094−3101

confirmed by the NMR spectroscopic method (Figure S2, Supporting Information). The rise of absorbance at 875 nm due to $[Fe^{IV}(O)(N4Py)]^{2+}$ in the reaction of $[Fe^{III}(OH)(N4Py)]^{2+}$ (0.50 mM) with 1 equiv of $[Ru^{III}(bpy)_3]^{3+}$ in the presence of a large excess of $TsO^-$ (5.0−20 mM) (Figure 2a) obeyed second-order kinetics (see the second-order plot in the inset).

The observed second-order rate constant ($k_{obs}$) increased linearly with increasing concentration of $TsO^-$ (Figure 2b). The kinetic formulation was also confirmed under pseudo-first-order conditions of $[Fe^{III}(OH)(N4Py)]^{2+}$ with a large excess of $[Ru^{III}(bpy)]^{3+}$ and $TsO^-$ (Figure S3, Supporting Information). The $k_{obs}$ value also increased linearly with increasing concentration of $H_2O$ in the absence of an additional PA (Figure S4, Supporting Information, and Table 1). This

**Table 1. Rate Constants for PCET Oxidations of $[Fe^{III}(OH)(N4Py)]^{2+}$ by $[Ru^{III}(bpy)_3]^{3+}$ with Various PA**

| proton acceptor | $K_b$ | $k_{PA}$, $M^{-2}$ $s^{-1}$ | $k_{PA,D}$, $M^{-2}$ $s^{-1}$ | KIE |
|---|---|---|---|---|
| $CF_3COO^-$ [a] | $7.9 \times 10^{12}$ | $9.6 \times 10^3$ | $4.4 \times 10^3$ | 2.2 |
| $TsO^-$ [b] | $4.0 \times 10^8$ | $4.1 \times 10^3$ | $2.0 \times 10^3$ | 2.1 |
| $NsO^-$ [b] | $6.3 \times 10^6$ | $3.1 \times 10^3$ | $1.6 \times 10^3$ | 1.9 |
| $DNsO^-$ [c] | $1.0 \times 10^3$ | $2.3 \times 10^2$ | $1.7 \times 10^2$ | 1.3 |
| $TfO^-$ [c] | 5.0 | $2.1 \times 10$ | $1.7 \times 10$ | 1.2 |
| $H_2O$ | n.d.[d] | $6.1 \times 10^{-1}$ [e] | n.d.[d] | n.d.[d] |

[a] $K_b$ values in MeCN are taken from ref 22. [b] $K_b$ values in MeCN are taken from ref 23. [c] $K_b$ values in MeCN are taken from ref 24. [d] n.d.: not determined. [e] $k_{H2O}$.

indicates that $H_2O$ acts as not only an oxygen source but also a PA in formation of $[Fe^{IV}(O)(N4Py)]^{2+}$. Thus, the rate of PCET formation of $[Fe^{IV}(O)(N4Py)]^{2+}$ is given by eq 4, where $k_{obs} = k_{H2O}[H_2O] + k_{PA}[TsO^-]$, $k_{H2O}$ is the rate constant without PA, and $k_{PA}$ is the rate constant with PA.

$$d[Fe^{IV}(O)]/dt = (k_{H2O}[H_2O] + k_{PA}[TsO^-]) \times [Fe^{III}(OH)][Ru^{III}] \quad (4)$$

PCET formation of $[Fe^{IV}(O)(N4Py)]^{2+}$ was also accelerated by other PA [$CF_3COO^-$, $NsO^-$ ($o$-$O_2N$-$C_6H_4SO_3^-$), $DNsO^-$ (2,4-$(O_2N)_2$-$C_6H_3SO_3^-$), and $TfO^-$ ($CF_3SO_3^-$)] (Figures 3 and 4).[23−25] $k_{PA}$ values were determined for other PA, and results are listed in Table 1 together with the basicity values of the PA employed ($K_b$).[26]

When $H_2O$ was replaced by $D_2O$ in PCET formation of $[Fe^{IV}(O)(N4Py)]^{2+}$ in the presence of $TsO^-$, a deuterium kinetic isotope effect (KIE = 2.1) was observed as shown in Figure 2b and Figure S5, Supporting Information. Reactions in the presence of other PA were also deterred by replacement of $H_2O$ by $D_2O$. KIE values were determined from comparison of the slope of $k_{obs}$ or pseudo-first-order rate constant ($k'_{obs}$) dependence on the concentration of PA ($k_{PA}$ and $k_{PA,D}$) in the presence of 0.56 M $H_2O$ and $D_2O$.

In the presence of 50 mM $CF_3COO^-$, which has the largest $K_b$ value among PA examined in this study, the $k_{obs}$ value is 390-fold larger than the value in the absence of $CF_3COO^-$.[27] In the case of $CF_3COO^-$, however, a plot of $k'_{obs}$ vs $[CF_3COO^-]$ exhibits a saturation behavior (Figure 3c).

Such a saturation behavior in Figure 3c may be explained by a change in the rate-determining step from proton transfer from $[Fe^{III}(OH)(N4Py)]^{2+}$ to $CF_3COO^-$ to electron transfer from $[Fe^{III}(O)(N4Py)]^+$, which is produced by deprotonation with a strong base ($CF_3COO^-$) to $[Ru(bpy)_3]^{3+}$. Alternatively the rate-determining step may be changed to electron transfer from

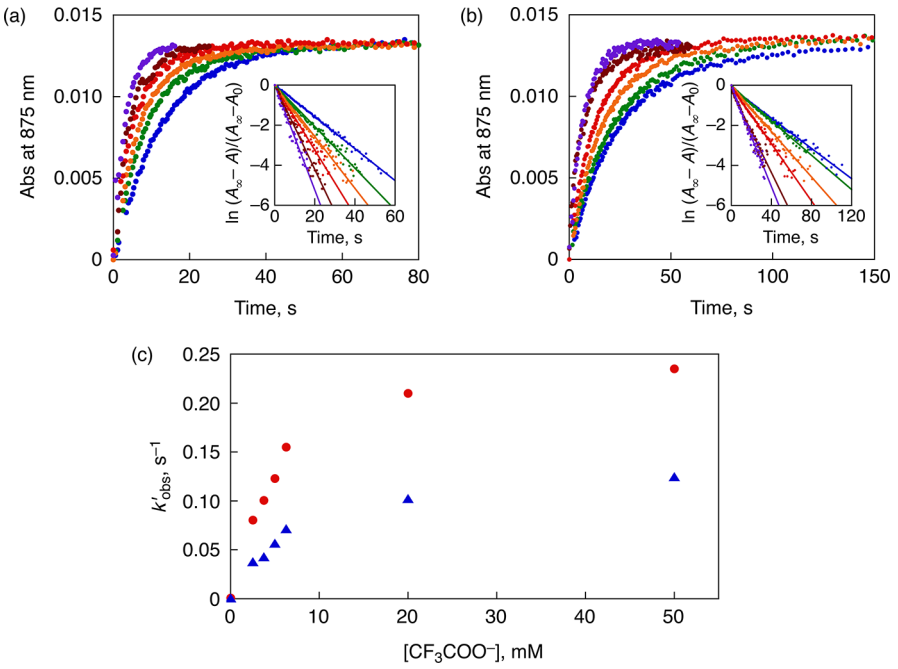


**Figure 3.** Time courses of absorbance changes at 875 nm due to $[Fe^{IV}(O)(N4Py)]^{2+}$ produced by PCET oxidation of $[Fe^{III}(OH)(N4Py)]^{2+}$ (0.25 mM) with $[Ru^{III}(bpy)_3]^{3+}$ (2.5 mM) in MeCN containing 0.56 M (a) $H_2O$ and (b) $D_2O$ in the presence of $CF_3COO^-$ (blue, 2.5 mM; green, 3.8 mM; orange, 5.0 mM; red, 6.3 mM; brown, 20 mM; purple, 50 mM) at 298 K, respectively. (Insets) Pseudo-first-order plots of the spectral changes in the reaction observed at 875 nm. $A_0$, $A_\infty$, and $A$ represent initial and final absorbance at 875 nm and absorbance at 875 nm during the reactions, respectively. (c) Plots of the pseudo-first-order rate constant ($k'_{obs}$) vs $[CF_3COO^-]$ for reactions in MeCN containing 0.56 M $H_2O$ (red) and $D_2O$ (blue).


dx.doi.org/10.1021/ic302573x | Inorg. Chem. 2013, 52, 3094−3101

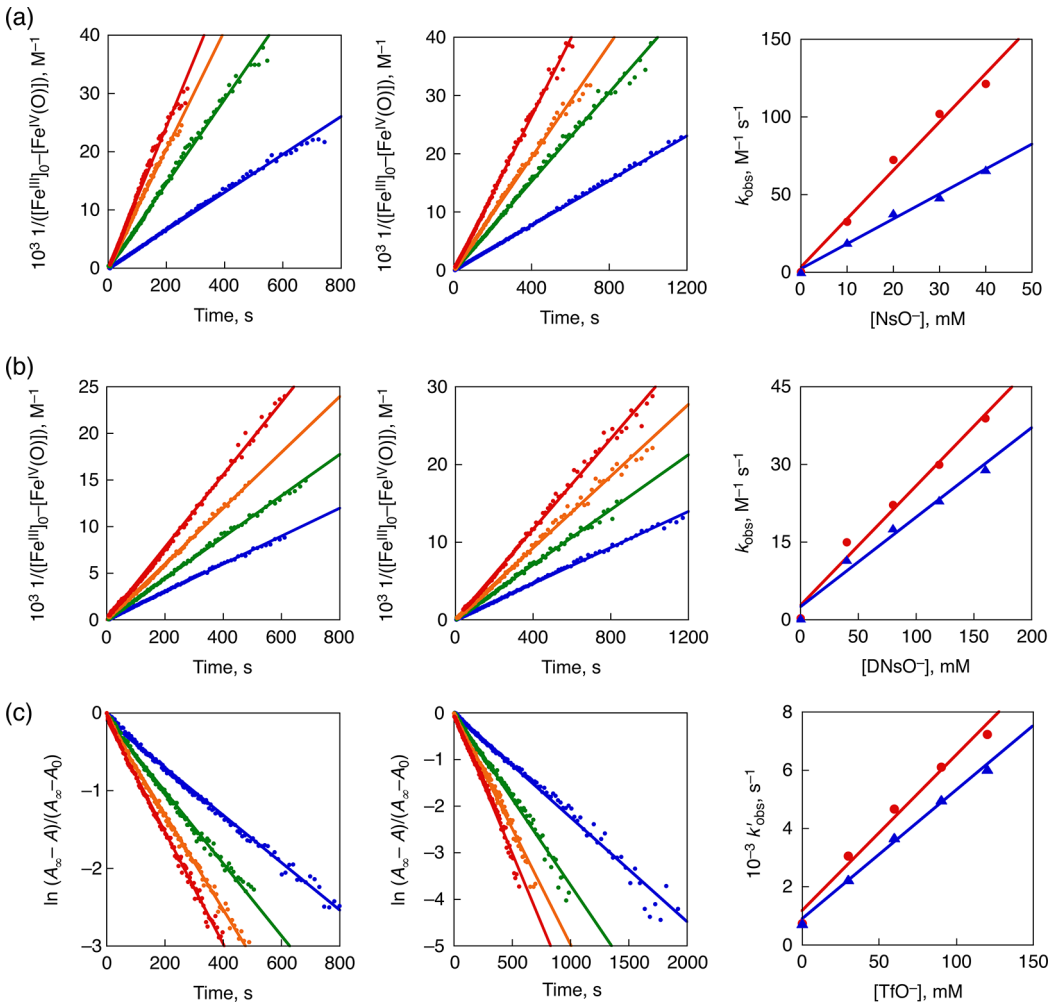


**Figure 4.** (Left and middle) Second-order plots of time traces of the absorption band at 875 nm due to $[Fe^{IV}(O)(N4Py)]^{2+}$ observed in PCET oxidation of $[Fe^{III}(OH)(N4Py)]^{2+}$ (0.25 mM) with $[Ru^{III}(bpy)_3]^{3+}$ (0.25 mM) in the presence of (a) $NsO^-$ (10−40 mM) and (b) $DNsO^-$ (40−160 mM); (c) first-order plots of the time traces in PCET oxidation of $[Fe^{III}(OH)(N4Py)]^{2+}$ (0.25 mM) with $[Ru^{III}(bpy)_3]^{3+}$ (2.5 mM) in the presence of $TfO^-$ (30−120 mM) in MeCN containing 0.56 M $H_2O$ (left) and $D_2O$ (middle) in MeCN at 298 K. (Right) Dependence of the pseudo-second-order rate constant ($k_{obs}$) for reactions on (a) $[NsO^-]$ and (b) $[DNsO^-]$; (c) dependence of pseudo-first-order rate constant ($k'_{obs}$) on $[TfO^-]$ in MeCN containing 0.56 M $H_2O$ (red) and $D_2O$ (blue).

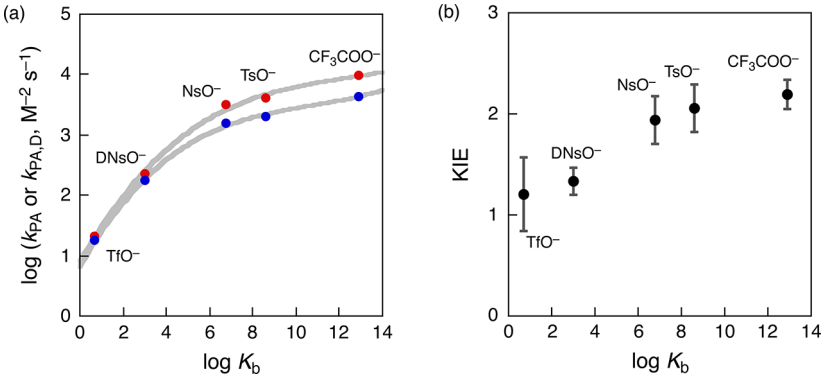


**Figure 5.** (a) Plots of log $k_{PA}$ and $k_{PA,D}$ for reaction between $[Fe^{III}(OH)(N4Py)]^{2+}$ and $[Ru^{III}(bpy)_3]^{3+}$ vs log $K_b$ performed in the presence of PA and 0.56 M $H_2O$ (red) and $D_2O$ (blue) in MeCN at 298 K. (b) Plots of KIE vs log $K_b$. KIE values are determined by dividing $k_{PA}$ by $k_{PA,D}$.

$[Fe^{III}(OH)(N4Py)]^{2+}$ to $[Ru(bpy)_3]^{3+}$, followed by fast depotonation of $[Fe^{IV}(OH)(N4Py)]^{3+}$ with $CF_3COO^-$ at large concentrations. In both cases, the KIE value would be changed to unity at the saturated stage. However, the KIE value remains constant even at the saturated stage in Figure 3c. Thus, the saturation behavior in Figure 3c may result from binding of $CF_3COO^-$ to the iron(III) species, where the rate-determining step of the reaction is changed to dissociation of $CF_3COO^-$. In fact, the EPR spectrum of the iron(III) complex in the presence of 10 mM $CF_3COO^-$ showed a different signal from that in the


dx.doi.org/10.1021/ic302573x | Inorg. Chem. 2013, 52, 3094−3101

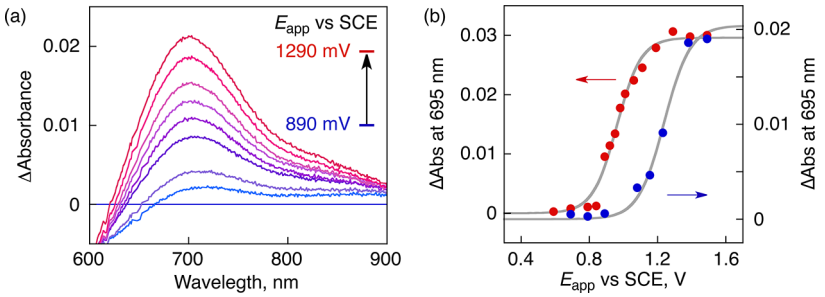


**Figure 6.** (a) Differential spectral changes of $[Fe^{III}(OH)(N4Py)]^{2+}$ solution (0.20 mM) on applying electric potential ($E_{app}$) (0.89−1.29 V vs SCE) in the presence of $H_2O$ (0.56 M) and $TsO^-$ (10 mM) in MeCN at 298 K. (b) Plots of differential absorption change vs applied potential in the absence (blue) and presence of $TsO^-$ (red) (10 mM).

absence of $CF_3COO^-$ (see Figure S1, Supporting Information). Because the concentration of $[Fe^{III}(OH)(N4Py)]^{2+}$ ($[Fe^{III}(OH)]$) is equal to $[Fe^{III}(OH)]_0/(1 + K[CF_3COO^-])$, where $[Fe^{III}(OH)]_0$ is the concentration without $CF_3COO^-$ and $K$ is the equilibrium constant of formation of $[Fe^{III}(CF_3COO^-)]$, $k'_{obs}$ is given by eq 5

$$k'_{obs} = k_{PA}[CF_3COO^-][Ru^{III}]/(1 + K[CF_3COO^-]) \quad (5)$$

which agrees with the experimental observation in Figure 3c. In this case, the $k_{PA}$ value was determined from the slope of a plot of $k'_{obs}$ vs $[CF_3COO^-]$ in the range of 0−6.0 mM, where a linear correlation was maintained.

The $k_{PA}$ value increases with increasing $K_b$ value of the proton acceptors to approach a constant value as shown in Figure 5a, where log $k_{PA}$ values are plotted against log $K_b$ values. The KIE value also increased with an increase in log $K_b$ (Figure 5b).[28] Observation of KIE suggests that O−H bond cleavage of $[Fe^{III}(OH)(N4Py)]^{2+}$ is involved in the rate-determining step of PCET formation of $[Fe^{IV}(O)(N4Py)]^{2+}$.

Remarkable acceleration effects of PA on PCET formation of $[Fe^{IV}(O)(N4Py)]^{2+}$ may result from the change in the one-electron oxidation potential ($E_{ox}$) of $[Fe^{III}(OH)(N4Py)]^{2+}$ in the presence of PA. Thus, we determined the $E_{ox}$ values of $[Fe^{III}(OH)(N4Py)]^{2+}$ in the absence and presence of $TsO^-$ by spectropotentiometic titration. Figure 6a shows the differential absorption change of $[Fe^{III}(OH)(N4Py)]^{2+}$ solution observed by changing the applied potential. $E_{ox}$ values in the absence and presence of $TsO^-$ (10 mM) in MeCN containing 0.56 M $H_2O$ have been determined by fitting the plots of absorbance change at 695 nm (Figure 6b) using the Nernst equation.[29,30] The best fits of the plots (solid gray lines in Figure 6b) afford $E_{ox}$ values of 1.24 and 0.96 V vs SCE in the absence and presence of $TsO^-$, respectively. The $E_{ox}$ value of $[Fe^{III}(OH)(N4Py)]^{2+}$ in MeCN containing $H_2O$ (0.56 M) without an additional PA is comparable to the reported value by Collins and co-workers in MeCN containing $H_2O$ (1.0 M).[30] The negative shift of 0.28 V in the presence of $TsO^-$ is attributed to stabilization of proton released in the oxidation of $[Fe^{III}(OH)(N4Py)]^{2+}$ by the proton acceptor. The $E_{ox}$ value of $[Fe^{III}(OH)(N4Py)]^{2+}$ (0.96 V vs SCE) in the presence of $TsO^-$ (10 mM) is still more positive than the one-electron reduction potential of $[Fe^{IV}(O)(N4Py)]^{2+}$ in the absence of proton source ($E_{red}$ = 0.51 V vs SCE)[27] because of the protonation of $[Fe^{III}(O)(N4Py)]^+$ by TsOH.[31] Such shift of the redox potential by assisting protonation/deprotonation by changing pH values of aqueous solutions have been reported in other systems.[13,17a,18] PCET formation of $[Fe^{IV}(O)(N4Py)]^{2+}$ becomes thermodynamically more favorable by 0.28 eV in the presence of $TsO^-$ (10 mM), resulting in 160-fold acceleration of the PCET rate.[33]

The kinetic results obtained in this study provide valuable insights into the mechanism of proton-acceptor-enhanced PCET oxidation of $[Fe^{III}(OH)(N4Py)]^{2+}$ with $[Ru^{III}(bpy)_3]^{3+}$ to produce $[Fe^{IV}(O)(N4Py)]^{2+}$ (vide infra). PCET pathways are generally divided into three cases: (1) an electron transfer followed by a proton transfer (ET/PT), (2) a proton transfer followed by an electron transfer (PT/ET), or (3) a concerted proton−electron transfer (CPET, where the proton moves to the proton acceptor and the electron moves from the iron(III) complex to the ruthenium(III) complex in a single kinetic step) as shown in Scheme 3.[34] If proton transfer from $[Fe^{III}(OH)(N4Py)]^{2+}$ to PA occurred first in the rate-determining step and that was followed by fast electron transfer from $[Fe^{III}(O)(N4Py)]^+$ to $[Ru^{III}(bpy)_3]^{3+}$ (PT/ET in Scheme 3), the rate of formation $[Fe^{IV}(O)(N4Py)]^{2+}$ would be independent of the concentration of $[Ru^{III}(bpy)_3]^{3+}$. Alternatively, if electron transfer from $[Fe^{III}(OH)(N4Py)]^{2+}$ to $[Ru^{III}(bpy)_3]^{3+}$ occurred first in the rate-determining step and that was followed by fast proton transfer from $[Fe^{IV}(OH)(N4Py)]^{3+}$ to PA (ET/PT in Scheme 3), the rate of formation $[Fe^{IV}(O)(N4Py)]^{2+}$ would be independent of the concentration of PA. Neither case agrees with the experimental observation in eq 4, where the rate is proportional to concentrations of both PA and $[Ru^{III}(bpy)_3]^{3+}$.

**Scheme 3. Mechanisms of Formation of $[Fe^{IV}(O)(N4Py)]^{2+}$ via PCET Oxidation of $[Fe^{III}(OH)(N4Py)]^{2+}$**

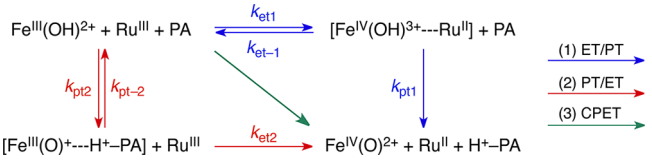


The first-order dependences of the rate on concentrations of both $[Ru^{III}(bpy)_3]^{3+}$ and PA together with the observation of KIE's (Figure 5) indicate that both electron transfer and proton transfer are involved in the rate-determining step or the equilibrium. If the initial electron transfer from $[Fe^{III}(OH)(N4Py)]^{2+}$ to $[Ru^{III}(bpy)_3]^{3+}$ is in an uphill equilibrium, followed by deprotonation of $[Fe^{IV}(OH)(N4Py)]^{3+}$, the rate of formation of $[Fe^{IV}(O)(N4Py)]^{2+}$ is given by eq 6

$$d[Fe^{IV}(O)]/dt = k_{pt1}K_{et}[Fe^{III}(OH)][PA] \quad (6)$$

where $k_{pt1}$ is the rate constant of proton transfer from $[Fe^{IV}(OH)(N4Py)]^{3+}$ to PA and $K_{et}$ is the electron-transfer equilibrium constant between $[Fe^{III}(OH)(N4Py)]^{2+}$ and


dx.doi.org/10.1021/ic302573x | Inorg. Chem. 2013, 52, 3094−3101

$[Ru^{III}(bpy)_3]^{3+}$ ($K_{et} = k_{et1}/k_{et-1}$). In such a case, the observed KIE in Figure 5b results from the proton transfer step from $[Fe^{IV}(OH)(N4Py)]^{3+}$ to PA, which must be exergonic to yield $[Fe^{IV}(O)(N4Py)]^{2+}$. Because the KIE of proton-transfer reactions is known to decrease with increasing driving force in the exergonic region,[35,36] the increasing KIE with increasing log $K_b$ in Figure 5b suggests that proton transfer is not the rate-determining step.

Alternatively, if the proton transfer from $[Fe^{III}(OH)(N4Py)]^{2+}$ to PA is an uphill equilibrium, followed by the rate-determining electron transfer from $[Fe^{III}(O)(N4Py)]^{+}$ to $[Ru^{III}(bpy)_3]^{3+}$, the rate of formation of $[Fe^{IV}(O)(N4Py)]^{2+}$ is given by eq 7

$$d[Fe^{IV}(O)]/dt = k_{et2}K_{pt}[Fe^{III}(OH)][PA] \quad (7)$$

where $k_{et2}$ is the rate constant of electron transfer from $[Fe^{III}(O)(N4Py)]^{+}$ to $[Ru^{III}(bpy)_3]^{3+}$ and $K_{pt}$ is the proton-transfer equilibrium constant between $[Fe^{III}(OH)(N4Py)]^{2+}$ and PA ($K_{pt} = k_{pt2}/k_{pt-2}$). In such a case, the observed KIE in Figure 5b results from the equilibrium deuterium isotope effect in $K_{pt}$. Typical deuterium isotope effects on the ionization constants of an acid ($H^+$−PA) at 298 K, $\Delta pK_a = pK_a(D^+-PA) - pK_a(H^+-PA)$, have been reported to range $0.2 < \Delta pK_a < 0.7$.[36] This corresponds to the isotope effects of 1.4−5.0. The observed KIE values in Figure 5b are within this range. The concerted proton- and electron-transfer (CPET) pathway can also explain the kinetic results in eq 4. In such a case, however, the KIE value would decrease with increasing driving force of proton transfer in the exergonic region.[37−39] Thus, the uphill proton-transfer equilibrium of $[Fe^{III}(OH)(N4Py)]^{2+}$ and PA followed by the rate-determining electron transfer from $[Fe^{III}(O)(N4Py)]^{+}$ to $[Ru^{III}(bpy)_3]^{3+}$ may be the most likely pathway for PCET formation of $[Fe^{IV}(O)(N4Py)]^{2+}$ with proton acceptors. In order to clarify the reason of a saturation behavior of log $k_{PA}$ vs log $K_b$ in Figure 5a as well as KIE vs log $K_b$ in Figure 5b, we need to examine and compare the PCET reactions of different $Fe^{III}$−OH complexes with various one-electron oxidants, which we plan to do in the next step.

## CONCLUSION

The rate of PCET oxidation of $[Fe^{III}(OH)(N4Py)]^{2+}$ by $[Ru^{III}(bpy)_3]^{3+}$ in MeCN containing water to produce $[Fe^{IV}(O)(N4Py)]^{2+}$ was remarkably accelerated by proton acceptors (PA). The acceleration rate increased with increasing basicity of PA, although the basicity of PA employed in this study is limited because of the instability of the one-electron oxidant, $[Ru^{III}(bpy)_3]^{3+}$, in the presence of a strong base.[26] This study provides new and valuable insights into PCET formation of $M^{(n+2)+}$=O.[40]

## EXPERIMENTAL SECTION

**Materials.** All solvents and chemicals were of reagent-grade quality, obtained commercially and used without further purification, unless otherwise noted. Acetonitrile (MeCN) was dried according to published procedures and distilled under Ar prior to use.[41] Tetramethylammonium hydroxide (TMAOH), trifluoroacetic acid (TFA), *p*-toluenesulfonic acid (TsOH), 3-nitrobenzenesulfonic acid (NsOH), 2,4-dinitrobenzenesulfonic acid (DNsOH), and trifluoromethanesulfonic acid (TfOH) were purchased from Tokyo Chemical Industry Co., Ltd. $D_2O$ (99.9% D) was purchased from Cambridge Isotope Laboratories. Hydrogen peroxide (35%) was purchased from Kishida Chemical Co., Ltd. They were used without further purification. All PA were prepared by neutralizing above acids with TMAOH in methanol at room temperature. Salts were purified by recrystallization by slow vapor diffusion of diethyl ether into methanol solutions of the salts. $[Fe^{II}(N4Py)(NCMe)](ClO_4)_2$, $[Fe^{III}(OH)(N4Py)]^{2+}$, and $[Fe^{IV}(O)(N4Py)]^{2+}$ were prepared by literature methods.[21,22,42] Iodosylbenzene (PhIO), $[Ru^{II}(bpy)_3](PF_6)_2$, and $[Ru^{III}(bpy)_3](PF_6)_3$ were prepared according to published procedures.[43,44]

**Kinetic Measurements.** Electron transfer (ET) from $[Fe^{III}(OH)(N4Py)]^{2+}$ to $[Ru^{III}(bpy)_3]^{3+}$ was examined at 298 K using a Hewlett-Packard 8453 photodiode-array spectrometer with a quartz cuvette (path length = 1.0 cm) or a UNISOKU RSP-601 stopped-flow spectrometer equipped with a MOS-type highly sensitive photodiode array. Generally, in the experiments to determine the pseudo-second-order rate constant, $[Fe^{III}(NCMe)(N4Py)]^{2+}$ was produced first by one-electron oxidation of $[Fe^{II}(NCMe)(N4Py)]^{2+}$ with 1 equiv of $[Ru^{III}(bpy)_3]^{3+}$ in dry MeCN. $H_2O$ (0.56 M) and a large excess of PA ($TsO^-$, $NsO^-$, or $DNsO^-$) were added into the solution to form $[Fe^{III}(OH)(N4Py)]^{2+}$. Then another equivalent of $[Ru^{III}(bpy)_3]^{3+}$ was added into the solution to start kinetic measurements. The pseudo-second-order rate constants ($k_{obs}$) for ET were determined by the second-order plots of the absorption changes observed at 875 nm due to $[Fe^{IV}(O)(N4Py)]^{2+}$ and the extinction coefficient of the complex at 875 nm (60 $M^{-1}$ $cm^{-1}$). Kinetic measurements to obtain pseudo-first-order rate constants ($k'_{obs}$) for the ET reaction were started by addition of $[Fe^{II}(NCMe)(N4Py)]^{2+}$ into the MeCN solution of 11 equiv of $[Ru^{III}(bpy)_3]^{3+}$ and excess amount of PA and 0.56 M of $H_2O$. Because formation of $[Fe^{III}(OH)(N4Py)]^{2+}$ was finished immediately (<1.0 s), the ET from $[Fe^{III}(OH)(N4Py)]^{2+}$ to $[Ru^{III}(bpy)_3]^{3+}$ proceeded under simple pseudo-first-order reaction conditions. $k'_{obs}$ values in the absence of PA and presence of $CF_3COO^-$, $TsO^-$, or $TfO^-$ at 298 K were determined by the first-order plots of the spectral changes observed at 875 nm.

**EPR Measurements.** Resulting solutions of ET from $[Fe^{II}(NCMe)(N4Py)]^{2+}$ ($1.0 \times 10^{-3}$ M) to $[Ru(bpy)_3]^{3+}$ ($1.0 \times 10^{-3}$ M) in the presence of $TsO^-$ ($1.0 \times 10^{-2}$ M) or $CF_3COO^-$ ($1.0 \times 10^{-2}$ M) or oxidation of $[Fe^{II}(NCMe)(N4Py)]^{2+}$ ($1.25 \times 10^{-3}$ M) by 0.5 equiv of $H_2O_2$ in MeCN in quartz EPR tubes (3.0 mm i.d.) were frozen at 77 K after deaeration. EPR spectra were taken on a JEOL X-band spectrometer (JES-RE1XE) under nonsaturating microwave power conditions (1.00 mW) operating at 9.2025 GHz. The magnitude of the modulation was chosen to optimize the resolution and the signal-to-noise ratio (S/N) of the observed spectra (modulation width, 10 G; modulation frequency, 100 kHz). *g* values were calibrated using an $Mn^{2+}$ marker.

**Spectroelectrochemical Experiments.** UV−vis spectroelectrochemical experiments were performed with an ALS630B electrochemical analyzer and a Hewlett-Packard 8453 photodiode-array spectrometer in MeCN containing 0.10 M $Bu_4NPF_6$ as a supporting electrolyte at 298 K in a cuvette (path length of 10 mm). A working electrode was 100 ppi porous reticulated vitreous carbon (BAS Inc.) cut to 10 mm × 9 mm × 20 mm so as to fit into the cuvette with electrical contact by means of a Pt wire.[32] Another Pt wire was used as a counter electrode. Potential was applied with respect to an Ag/$AgNO_3$ (10.0 mM) reference electrode. All potentials (vs $Ag/Ag^+$) were converted to values vs SCE by adding 0.29 V.[45]

**$^1$H NMR Measurement.** $^1$H NMR spectra were measured after ET oxidation of $[Fe^{III}(OH)(N4Py)]^{2+}$ by $[Ru^{III}(bpy)_3]^{3+}$ in MeCN-$d_3$ containing $D_2O$ (0.56 M) and $TfO^-$ ($1.0 \times 10^2$ mM) or oxidation of $[Fe^{II}(NCMe)(N4Py)]^{2+}$ by 1.2 equiv of PhIO in MeCN-$d_3$ (blue) in NMR tubes at 298 K with a JEOL JNM-AL300 (300 MHz) NMR spectrometer.

## ASSOCIATED CONTENT

### Supporting Information

EPR spectra of $[Fe^{III}(OH)(N4Py)]^{2+}$ (Figure S1), NMR spectrum of $[Fe^{IV}(O)(N4Py)]^{2+}$ generated (Figure S2), and kinetic analyses Figures S1−S5. This material is available free of charge via the Internet at http://pubs.acs.org.


dx.doi.org/10.1021/ic302573x | *Inorg. Chem.* 2013, 52, 3094−3101

## AUTHOR INFORMATION


### Corresponding Author

*E-mail: wwnam@ewha.ac.kr (W.N.); fukuzumi@chem.eng.osaka-u.ac.jp (S.F.).


### Notes

The authors declare no competing financial interest.

## ACKNOWLEDGMENTS


The work at OU was supported by a Grant-in-Aid (20108010) by MEXT, Japan (to S.F.), and the research at EWU was supported by KRF/MEST of Korea through CRI (to W.N.), GRL (2010-00353) (to W.N.), and WCU (R31-2008-000-10010-0) (to S.F. and W.N.). Y.M. appreciates support from a JSPS fellowship for young scientists.


## REFERENCES


(1) (a) Stewart, R. *Oxidation Mechanisms*; Benjamin: New York, 1964. (b) Mijs, W. J.; De Jonge, C. R. H. I. *Organic Synthesis by Oxidation with Metal Compounds*; Plenum: New York, 1986. (c) Sheldon, R. A.; Kochi, J. K. *Metal-Catalyzed Oxidations of Organic Compounds*; Academic Press: New York, 1981. (d) Nugent, W. A.; Mayer, J. M. *Metal−Ligand Multiple Bonds*; Wiley: New York, 1988. (e) Meunier, B. *Biomimetic Oxidations Catalyzed by Transition Metal Complexes*; Imperial College Press: London, 1998. (f) Punniyamurthy, T.; Velusamy, S.; Iqbal, J. *Chem. Rev.* **2005**, *105*, 2329.

(2) (a) Sono, M.; Roach, M. P.; Coulter, E. D.; Dawson, J. H. *Chem. Rev.* **1996**, *96*, 2841. (b) Harris, D. L.; Loew, G. H. *J. Am. Chem. Soc.* **1998**, *120*, 8941. (c) P. R. Ortiz de Montellano, *Cytochrome P450: Structure, Mechanism, and Biochemistry*, 3rd ed.; Kluwer Academic/Plenum: New York, 2004. (d) Meunier, B.; de Visser, S. P.; Shaik, S. *Chem. Rev.* **2004**, *104*, 3947. (e) Denisov, I. G.; Makris, T. M.; Sligar, S. G.; Schlichting, I. *Chem. Rev.* **2005**, *105*, 2253.

(3) (a) Holm, R. H. *Chem. Rev.* **1987**, *87*, 1401. (b) Shilov, A. E.; Shul'pin, G. B. *Chem. Rev.* **1997**, *97*, 2879. (c) Balcells, D.; Clot, E.; Eisenstein, O. *Chem. Rev.* **2010**, *110*, 749. (d) Gunay, A.; Theopold, K. H. *Chem. Rev.* **2010**, *110*, 1060.

(4) In *Metal-Oxo and Metal-Peroxo Species in Catalytic Oxidations*; Meunier, B., Ed.; Springer-Verlag: Berlin, 2000.

(5) Kovacs, J. A. *Science* **2009**, *299*, 1024.

(6) (a) Krebs, C.; Fujimori, D. G.; Walsh, C. T.; Bollinger, J. M., Jr. *Acc. Chem. Res.* **2007**, *40*, 484. (b) Kovaleva, E. G.; Lipscomb, J. D. *Nat. Chem. Biol.* **2008**, *3*, 186.

(7) McEvoy, J. P.; Brudvig, G. W. *Chem. Rev.* **2006**, *106*, 4455.

(8) OEC Architecture of the Photosynthetic Oxygen-Evolving Center, see: (a) Ferreira, K. N.; Iverson, T. M.; Maghlaoui, K.; Barber, J.; Iwata, S. *Science* **2004**, *303*, 1831. (b) Loll, B.; Kern, J.; Saenger, W.; Zouni, A.; Biesiadka, J. *Nature* **2005**, *438*, 1040. (c) Umena, Y.; Kawakami, K.; Shen, J.-R.; Kamiya, N. *Nature* **2011**, *473*, 55.

(9) For a recent study to assign the primary proton acceptor in a bucket-brigade-type mechanism of proton transfer from OEC to outside of lumen as carboxylate anion form of D1-Asp-61, see: Siegbahn, P. E. M. *Phys. Chem. Chem. Phys.* **2012**, *14*, 4849.

(10) It should be noted that Scheme 1 has been one of several proposals and that other proposals exist as reported in ref 9.

(11) Lewis, N. S.; Nocera, D. G. *Prog. Natl. Acad. Sci. U.S.A.* **2006**, *103*, 15729.

(12) Fukuzumi, S.; Kishi, T.; Kotani, H.; Lee, Y.-M.; Nam, W. *Nature Chem.* **2011**, *3*, 38.

(13) Ohzu, S.; Ishizuka, T.; Hirai, Y.; Jiang, H.; Sakaguchi, M.; Ogura, T.; Fukuzumi, S.; Kojima, T. *Chem. Sci.* **2012**, *3*, 3241.

(14) Che, C.-M.; Yam, V. W.-W.; Mak, T. C. W. *J. Am. Chem. Soc.* **1990**, *112*, 2284.

(15) Low, D. W.; Winkler, J. R.; Gray, H. B. *J. Am. Chem. Soc.* **1996**, *118*, 117.

(16) Kotani, H.; Suenobu, T.; Lee, Y.-M.; Nam, W.; Fukuzumi, S. *J. Am. Chem. Soc.* **2011**, *133*, 3249.

(17) (a) Hirai, Y.; Kojima, T.; Mizutani, Y.; Shiota, Y.; Yoshizawa, K.; Fukuzumi, S. *Angew. Chem., Int. Ed.* **2008**, *47*, 5772. (b) Lee, Y.-M.; Dhuri, S. N.; Sawant, S. C.; Cho, J.; Kubo, M.; Ogura, T.; Fukuzumi, S.; Nam, W. *Angew. Chem., Int. Ed.* **2009**, *48*, 1803.

(18) Huynh, M. H. V.; Meyer, T. J. *Chem. Rev.* **2007**, *107*, 5004.

(19) For detailed kinetic analysis of PCET of phenol derivatives or a cobalt cluster, see: (a) Sjödin, M.; Styring, S.; Wolpher, H.; Xu, Y.; Sun, L.; Hammarström, L. *J. Am. Chem. Soc.* **2005**, *127*, 3855. (b) Markle, T. F.; Rhile, I. J.; Mayer, J. M. *J. Am. Chem. Soc.* **2011**, *133*, 17341. (c) Symes, M. D.; Surendranath, Y.; Lutterman, D. A.; Nocera, D. G. *J. Am. Chem. Soc.* **2011**, *133*, 5174.

(20) PCET formation of $[Fe^{IV}(O)(N4Py)]^{2+}$ in a mixed solvent of acetonitrile and acetate buffer solution (pH 5.0) was previously reported in ref 15.

(21) Kaizer, J.; Klinker, E. J.; Oh, N. Y.; Rohde, J.-U.; Song, W. J.; Stubna, A.; Kim, J.; Münck, E.; Nam, W.; Que, L., Jr. *J. Am. Chem. Soc.* **2004**, *126*, 472.

(22) Roelfes, G.; Lubben, M.; Chen, K.; Ho, R. Y. N.; Meetsma, A.; Genseberger, S.; Hermant, R. M.; Hage, R.; Mandal, S. K.; Young, V. G.; Zang, Y.; Kooijman, H.; Spek, A. L.; Que, L., Jr.; Feringa, B. L. *Inorg. Chem.* **1999**, *38*, 1929.

(23) p*K*a for $CF_3COOH$; see: Anne, A.; Morioux, J.; Savéant, J. M. *J. Am. Chem. Soc.* **1993**, *115*, 10224.

(24) p*K*a for TsOH and NsOH; see: Kütt, A.; Leito, I.; Kajurand, I.; Sooväli, L.; Vlasov, V. M.; Yagupolskii, L. M.; Koppel, I. A. *J. Org. Chem.* **2006**, *71*, 2829.

(25) p*K*a for DNsOH and TfOH; see: Kütt, A.; Rodima, T.; Saame, J.; Raamat, E.; Mäemets, V.; Kaljurand, I.; Koppel, A.; Garlyauskayte, R. Y.; Yagupolskii, Y. L.; Yagupolskii, L. M.; Bernhardt, E.; Willner, H.; Leito, I. *J. Org. Chem.* **2011**, *76*, 391.

(26) $[Ru^{III}(bpy)]^{3+}$ was not stable in the presence of stronger base than $CF_3COO^-$, e.g., $CH_3COO^-$.

(27) The acidity of Brønsted acids in MeCN has been reported in refs 22−24. Because we used anions of relatively strong acids, the effect of water molecules is expected to be much smaller as compared with anions of weak acids. Thus, the reported $K_b$ (or $K_a$) values in MeCN are accurate enough to discuss the dependence of $k_{PA}$ on $K_b$ of different anions of strong acids.

(28) For the dependence of KIE value on the p$K_b$ value of proton acceptor, see: Dixon, J. E.; Bruice, T. C. *J. Am. Chem. Soc.* **1970**, *92*, 905.

(29) Lee, Y.-M.; Kotani, H.; Suenobu, T.; Nam, W.; Fukuzumi, S. *J. Am. Chem. Soc.* **2008**, *130*, 434.

(30) Because the spectral change observed in Figure 6a was not completely reversible, the $E_{1/2}$ values in Figure 6b should be regarded as apparent $E_{ox}$ values under the present electrochemical oxidation conditions.

(31) Collins, M. J.; Ray, K.; Que, L., Jr. *Inorg. Chem.* **2006**, *45*, 8009.

(32) Wang, D.; Zang, M.; Bühlmann, P.; Que, L., Jr. *J. Am. Chem. Soc.* **2010**, *132*, 7638.

(33) In this case, about 46% of the free energy change is reflected in the activation free energy, because 160-fold acceleration of the PCET rate corresponds to 0.13 eV in terms of activation free energy.

(34) Warren, J. J.; Tronic, T. A.; Mayer, J. M. *Chem. Rev.* **2010**, *110*, 6961.

(35) Fukuzumi, S.; Koumitsu, S.; Hironaka, K.; Tanaka, T. *J. Am. Chem. Soc.* **1987**, *109*, 305.

(36) Cohen, A. O.; Marcus, R. A. *J. Phys. Chem.* **1968**, *72*, 4249.

(37) (a) Erickson, K. M.; Arcis, H.; Raffa, D.; Zimmerman, G. H.; Tremaine, P. R. *J. Phys. Chem. B* **2011**, *115*, 3038. (b) Jancso, G.; Van Hook, W. A. *Chem. Rev.* **1974**, *74*, 689.

(38) (a) Pryor, W. A.; Kneipp, K. G. *J. Am. Chem. Soc.* **1971**, *93*, 5584. (b) Ishikawa, M.; Fukuzumi, S. *J. Chem. Soc., Faraday Trans.* **1990**, *86*, 3531.

(39) Judging from the small KIE values, no tunneling is involved in the present case.

(40) For oxidation of $Mn^{IV}$−OH to form $Mn^{V}\equiv O$ in OEC, which is thought to proceed via PT/ET, see: Haumann, M.; Liebisch, P.; Müller, C.; Barra, M.; Grabolle, M.; Dau, H. *Science* **2005**, *310*, 1019.

(41) Armarego, W. L. F.; Chai, C. L. L. *Purification of Laboratory Chemicals*, 6th ed.; Pergamon Press: Oxford, 2009.
(42) Lubben, M.; Meetsma, A.; Wilkinson, E. C.; Feringa, B.; Que, L., Jr. *Angew. Chem., Int. Ed. Engl.* **1995**, *34*, 1512.
(43) DeSimone, R. E.; Drago, R. S. *J. Am. Chem. Soc.* **1970**, *92*, 2343.
(44) Saltzman, H.; Sharefkin, J. G. *Organic Syntheses*; Wiley: New York, 1973; Collect. Vol. *V*, p 658.
(45) Mann, C. K.; Barnes, K. K. *Electrochemical Reactions in Nonaqueous Systems*; Mercel Dekker: New York, 1970.